Actinide diffusion in zirconium and the role of oxidation

N. Bérerd, H. Catalette, A. Chevarier, H. Faust, N. Moncoffre

Actinide diffusion in zirconium and the role of oxidation
N. Bérerd[1], H. Catalette[2], A. Chevarier[1], N. Chevarier[1], H. Faust[3], **N. Moncoffre[1]**
[1]Institut de Physique Nucléaire de Lyon, IN2P3/CNRS, Université Claude Bernard, F-69622 Villeurbanne Cedex, France, [2] EDF, Les Renardières, Route de Sens, Ecuelles, 77818 Moret sur Loing, France,[3] Institut Laue-Langevin, B.P. 156, F-38042 Grenoble Cedex 9, France

Abstract

Nuclear fuel devices of Pressurised Water Reactors are composed of uranium oxide pellets which are enclosed in zircaloy cylinders. During reactor operation different processes occur. In the contact with the fuel the zircaloy oxidises nonuniformly in depths of order of some micrometers. Further on, energy deposition of fission recoils leads to sputtering of uranium onto the inner surface of the cladding material. Thus, sputtered uranium ions start to migrate outwards. This paper presents first the results of experiments performed on the Lohengrin spectrometer in order to simulate the alteration of cladding tubes in contact with the nuclear fuel during irradiation. The energy loss of selected fission products is correlated to an oxygen mass gain. From these experiments, we deduce the oxidation kinetics constant under irradiation at a mean temperature of 400°C. These results are compared with those of a thermal oxidation. Following oxidation the fission product kinetic energy is stabilised, but still a broadening of the energy distribution is observed, which is characteristic of actinide diffusion inside the zirconia target. Using the Fick model, an actinide diffusion coefficient into zirconia under irradiation is deduced.

Keywords: Irradiation, Oxidation, Diffusion

1. Introduction

Fuel cladding tubes of Pressurised Water Reactors have been subject to numerous investigations to understand their behaviour. The oxidation process on both sides of the zircaloy tubes has been in particular thoroughly characterised [1, 2]. The cladding tube inner surface is known to be oxidised by reduction of the UO_2 pellets which are in slight contact with the Zr cladding [3]. The oxidation kinetics during nuclear operation is subject to discussion as it depends on several conditions: temperature, residual oxygen pressure and irradiation conditions. In addition, fission products are implanted by recoil in this inner oxide layer and energy deposition of fission recoils leads to sputtering of uranium onto the inner surface of the cladding material. The as-sputtered uranium can then migrate outwards. It is of primary importance to determine the diffusion parameters of the fission products and actinides in the cladding. Consequently, this work will be presented into two parts. The first part is devoted to zirconium oxidation measurements in reactor conditions performed on the ILL (Institut Laue Langevin) neutron experimental reactor in Grenoble. The oxidation kinetics constant deduced from these experiments are compared to thermal oxidation measurements obtained in the same temperature and pressure conditions. The second part presents the study of uranium diffusion in the oxidised zirconium.

2. Experimental set up

  2.1 The ILL Lohengrin mass spectrometer

Zirconium oxidation and uranium diffusion in reactor conditions have been performed at the Lohengrin mass spectrometer. In the spectrometer beam tube, an uranium-oxide target stacked onto a Zr foil is placed in a high neutron flux of $5x10^{14}$ n cm^{-2} s^{-1}. Uranium is enriched in ^{235}U to about 99%. Fission rates of standard targets (50

to 100 µg. cm^{-2}) reach about 10^{11} particles s^{-1}. The high energetic fission products leaving the UO$_2$ target transverse a Zr foil of 2µm thickness and 3.5 cm^2 surface which is to be investigated and placed in front of the target. The fission fragments are analysed in mass and kinetic energy in two successive magnetic and electric fields respectively. The separated fragments are detected in a high resolution ionisation chamber [4]. The process of oxidation and diffusion can be detected by scanning over the kinetic energy distribution of a selected fission product mass at successive times. The kinetic energy evolution of A=90 and Q=18 selected fission fragments is presented in figure 1. In experimental configuration, the Zr foil is heated by the γ radiation from the ILL reactor and by the fission fragments from the UO$_2$ target which are slowed down in the foil. Taking into account the γ heating in the in-pile position (about 0.6 W g^{-1}) and the heating by the fission product (45 MeV energy loss per fragment), the temperature of the Zr foil is of the order of 400°C with an error of about 25% [5]. The estimated partial oxygen pressure inside the beam tube is around 10^{-5} mbar.

2.2 Coupling of thermal annealing and RBS analysis

The zirconium thermal oxidation has been investigated at an oxygen partial pressure of 10^{-5} mbar and at a 400°C temperature. Samples are placed inside a stainless steel tube. Vacuum is obtained thanks to a turbomolecular pumping and adjusted by using a dry air variable leak valve. The furnace temperature is regulated at ±3°C and controlled by a thermocouple. For each annealing time, zirconium oxidation is measured by Rutherford Backscattering experiments performed using 1 MeV α particles. At this incident α energy the sensitivity is about 5x10^{16} oxygen atoms cm^{-2}. In figure 2 the RBS α yield on a non oxidised sample is compared to those of oxidised ones respectively after 2 and 18 hours annealing.

3. Results

3.1 Comparison between oxidation under irradiation and thermal oxidation

At ILL, we have performed systematic energy measurements as shown in figure 1. After an irradiation of 62 hours the complete oxidation of the zirconium foil has occurred which corresponds to an energy shift of 19.7 MeV of the selected A=90 fission product. From the experimental mean kinetics energy loss, the oxygen mass gain in the Zr foil was calculated by using the stopping tables for heavy ions in solids from Ziegler [6]. In the considered energy range corresponding to the oxidation process, the mean oxygen stopping power value is equal to 1195 eV/10^{15} at cm^{-2}. After the oxidation phase no more shift of the mean energy value is observed as shown in figure 3. At this stage, the whole foil is oxidised and the stoichiometry corresponds to ZrO$_2$.

The oxidation kinetics of zirconium under irradiation at 400°C is presented in figure 4. No parabolic evolution is noted which means that oxidation is not limited by the oxygen diffusion. This can be interpreted by the presence of numerous defects created by fission products. The slope of the straight line gives the kinetics constant to be equal to 1.5x10^{17} oxygen at cm^{-2} h^{-1}. This result needs to be compared to the kinetics constant of thermal zirconium oxidation in the same conditions of temperature and pressure (400°C and 10^{-5} mbar).

In thermal oxidation experiments the oxidised thickness is deduced for each annealing time from the fits of the RBS distributions. The results are presented in figure 4 (dotted line). It appears that the oxidation kinetics is much smaller compared to that under irradiation. The slope of this curve leads to a kinetics constant of 0.7x10^{17} oxygen at cm^{-2} h^{-1}. This factor 2 can be attributed to the defects induced by the fission product energy loss in the zirconium foil.

3.2 Uranium diffusion

After the oxidation phase, the fission product energy is stabilised but a broadening of the energy distributions is observed. Such an evolution is presented in figure 5. It is characteristic of the actinide diffusion inside the zirconia target. Within 240 hours, the half width of the almost gaussian energy distributions increases from 12.73 MeV to 17.27 MeV. An analysis of these data has been performed assuming a gaussian shape of the energetic distributions. The initial distribution is assumed to be the one after 62 hours of irradiation when the whole zirconium foil is oxidised and the final distribution is the last measurement (after 240 hours). We have simulated the uranium distribution evolution by subtracting the two distributions mentioned above. The resulting curve is then deconvoluted into 5 gaussian distributions dividing the surface region into 5 slices, the first one corresponding to the initial uranium distribution. The amplitude of each gaussian is considered as proportional to the uranium concentration whereas the energy is converted into depth of zirconia. An analytical solution of the Fick law is given by an erf function distribution of uranium. It is thus possible to reproduce the experimental data with a diffusion coefficient of uranium in zirconia equal to $2x10^{-16}$ cm^2 s^{-1}.

Conclusion

References

[1] C. Lemaignan and A. T. Motta: 'Zirconium alloys in nuclear applications', Materials and Technology, R. W. Cahn, P. Haasen, E. J. Kramer ed., 10B, (1994)

[2] B. Cox, : 'Oxidation of zirconium and its alloys', Advance in corrosion science and technology, Fontana and Staetile ed., New York, (5) 173 (1976)

[3] C. Lemaignan: Compte rendu DTP/SECC n096-010A, CEA- Grenoble (1996)

[4] J. P Bocquet, R. Brissot, H. R. Faust : Nucl. Instr. and Meth. in Phys. Res.B, A267, 466 (1988)

[5] H. Faust, A. Chevarier, N. Chevarier, J.C. Duclot, N. Millard-Pinard, N. Moncoffre : Intern. Workshop on Nuclear. Fission, Pont d'Oye, Belgium, Ed. By C. Wagemans, O. Serot, P. D'hondt, World Sc., Proc. 267 (1999)

[6] J. F. Ziegler: The stopping and Ranges of Ions in Matter, vol.5, Pergamon Press

Figure Captions

Figure 1 : Evolution of the energy distribution of fission products (A=90, Q=18) during 62 hours

Figure 2: RBS spectra obtained on a Zr foil (t=0) and after 2 thermal annealing (t=2h and t=18h)

Figure 3: Evolution of the maximum energy of fission products (A=90, Q=18) as function of time

Figure 4: Oxidation kinetics under irradiation (full line) or thermal oxidation (dashed line)

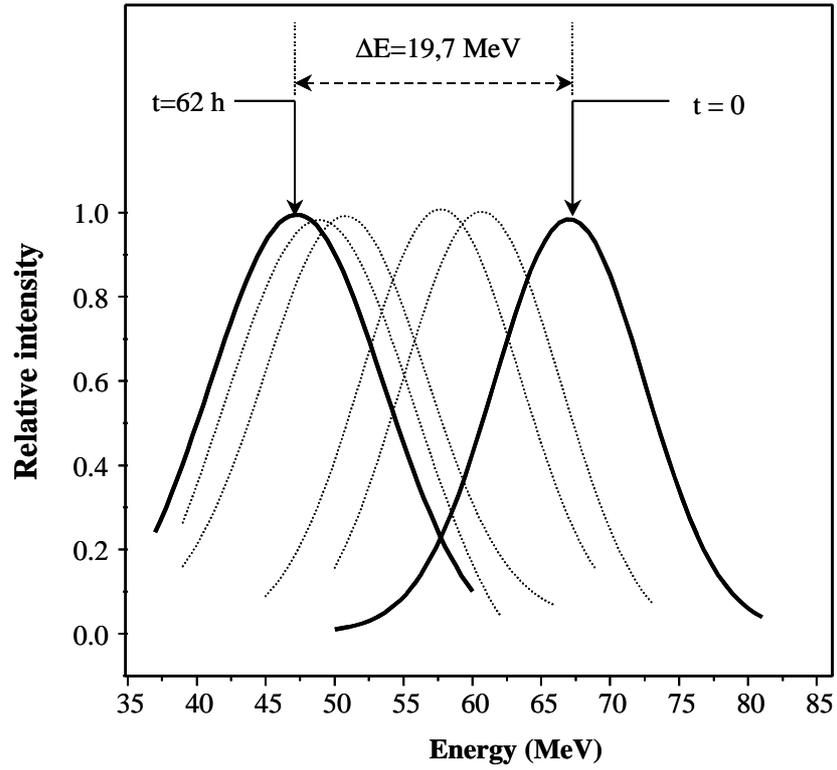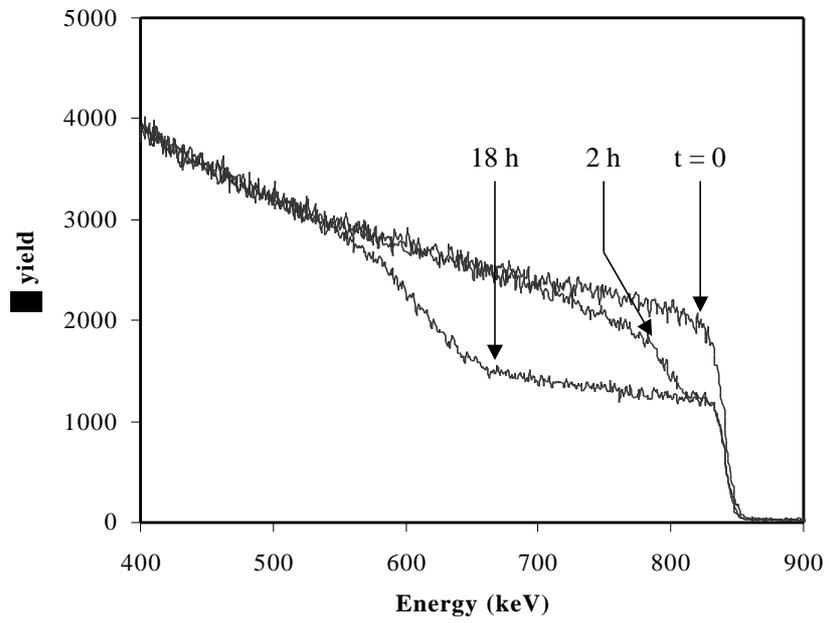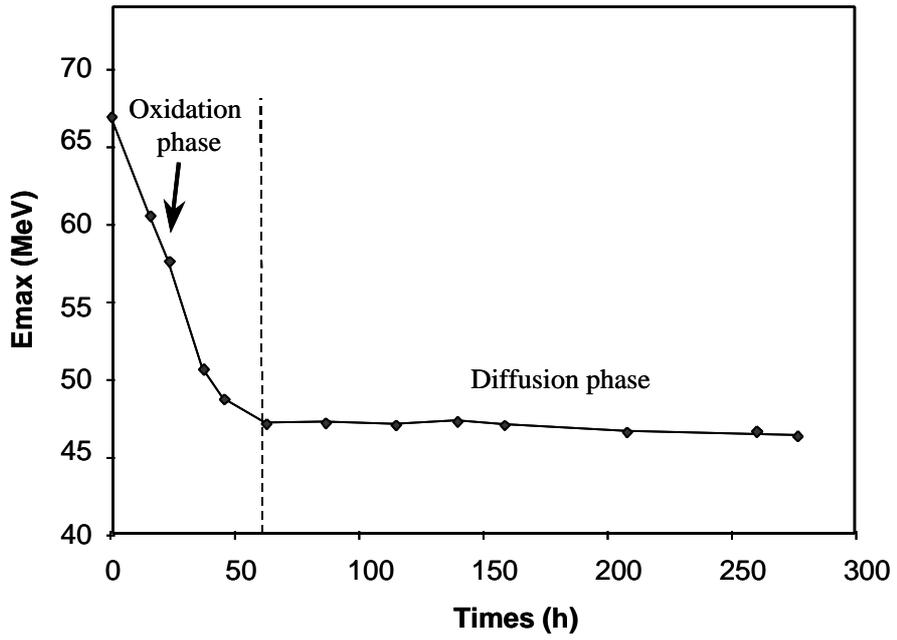**Figure 5:** Evolution of the energy distribution of fission products (A=90, Q=18) during the uranium diffusion phase
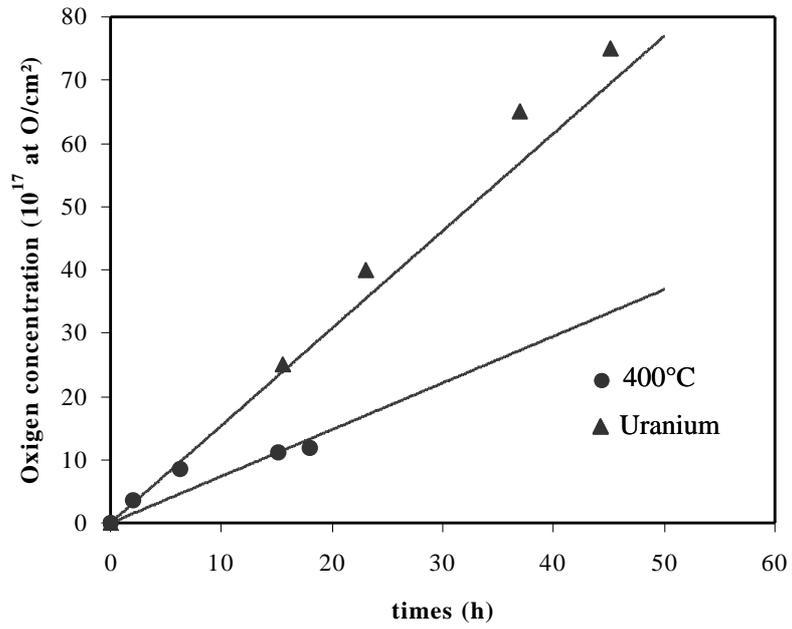
Figure 1

Figure 2

Figure 3

Figure 4

Figure 5